Modelling the Influences of Solid-State Interdiffusion and Dissolution on Transient Liquid Phase Sintering Kinetics in a Binary Isomorphous System

D.M. TURRIFF and S.F. CORBIN

A simple model was developed to predict the impact that solid-state interdiffusion and dissolution have on liquid formation and its duration during transient liquid phase sintering (TLPS). The model predicts that solid-state interdiffusion can dramatically reduce the amount of liquid initially formed during heating. This reduction is dependent on the heating rate and initial base metal particle size. In cases of sintering above the additive phase melting point, the model predicts that base metal dissolution increases liquid phase formation and that this additional melting reduces the base metal particle size. The model predicts that longer times are required to solidify isothermally the greater amounts of liquid formed at higher temperatures (because of dissolution). This agreed qualitatively with experimental results for a Ni-65 wt pct Cu TLPS mixture sintered at 1090 °C and 1140 °C. Quantitative comparisons between the model and experiment were good at 1140 °C; however, the rate of isothermal solidification was underestimated by the model for intermediate sintering times at 1085 °C.

I. INTRODUCTION

TRANSIENT liquid phase sintering (TLPS) has been used as a novel powder metallurgy (PM) process for forming bulk materials, ceramics, and composites.[1,2] Powder mixtures consisting primarily of a high melting point base metal powder (considered as constituent B) can be more easily sintered when in the presence of a low melting point additive powder (hereafter referred to as constituent A, the melting point depressant or solute phase).[1,2] Both constituents are typically in prealloyed or elemental powder form. A simple example of a TLPS mixture is based on the schematic binary isomorphous phase diagram in Figure 1. The typical temperature segments used in TLPS are shown as well.

The TLPS of powder mixtures depends on the formation of a liquid phase at the processing temperature (T_P) below the melting point of the base metal powder yet above that of the additive phase (T_A). The presence of the liquid enhances mass transport rates and densification (versus solid-state sintering) by exerting a capillary pull to rearrange powder particles.[1–3] This liquid isothermally solidifies over time by solute diffusion into the base metal particles as the T_P is held above T_A.

Figure 2 shows the different stages that have been identified in the TLPS process.[2,4] A TLPS mixture of pure A and B powders initially mixed to have a solute content does the following: (1) solid state sinters during the heating stage, leading to interdiffusion of additive and based metal atoms; (2) forms a liquid phase through the melting of phase A and (if $T > T_A$) through the dissolution of the B phase that spreads through the powder mixture and causes densification; (3) undergoes gradual isothermal solidification of the liquid at T_P by solute diffusion into the base metal particles to form a single solid phase eventually; and (4) homogenizes to eliminate compositional gradients. Base metal particle size (a_B), solute diffusivity (D) within the base metal powder, T_P, heating rate (R_H), and bulk solute content of the mixture (C_O) have been found to influence the amount of liquid formed significantly as well as the amount of time required for it to isothermally solidify.[4–11]

The advantages that TLPS offers over conventional solid-state sintering include rapid densification during sintering because of the capillary action and enhanced mass transport created by the liquid phase, lower sintering temperatures, and reduced microstructural coarsening attributable to shorter and lower temperature sintering. In addition, the advantage that TLPS offers over conventional liquid phase sintering, where the liquid is persistent, is that the liquid is ''removed'' from the microstructure before cooling, leading to a more homogeneous and higher strength compact. This removal of the transient liquid also has the advantage of creating a new solid alloy from an initial solid/liquid two-phase mixture, which exhibits an increased melting point after initial processing. This ''variable melting point'' (VMP) behavior is being used in the development of TLPS solder and brazing compounds[4–10] and in wide-gap transient liquid phase bonding (TLPB).[12,13]

The primary disadvantage of TLPS is that it is relatively sensitive to processing conditions.[14,15] This is primarily attributable to the variability in the volume of liquid generated during sintering. For a given composition, this liquid volume is determined by (1) the extent of interdiffusion between the additive and base metal phases while heating in the solid state and (2) the impact of the subsequent dissolution of the alloyed regions during heating past the additive phase melting point to the T_P. The solid-state interdiffusion and dissolution process are sensitive to R_H, powder size, peak T_P, and additive/base metal initial powder distribution.[8,11,14,15] This sensitivity can lead to variable liquid formation and sintered densities.

There is a considerable body of experimental work that has investigated the general problem of liquid phase sintering (LPS) of multielemental mixtures.[1–3,14–16] An excellent review of much of this work has been recently published by

D.M. TURRIFF, Graduate Student, and S.F. CORBIN, Associate Professor, are with the Department of Mechanical Engineering, University of Waterloo, 200 University Avenue, Waterloo, Ontario, Canada N2L 3G1. Contact e-mail: scorbin@mechengl.uwaterloo.ca

Manuscript submitted September 6, 2005.

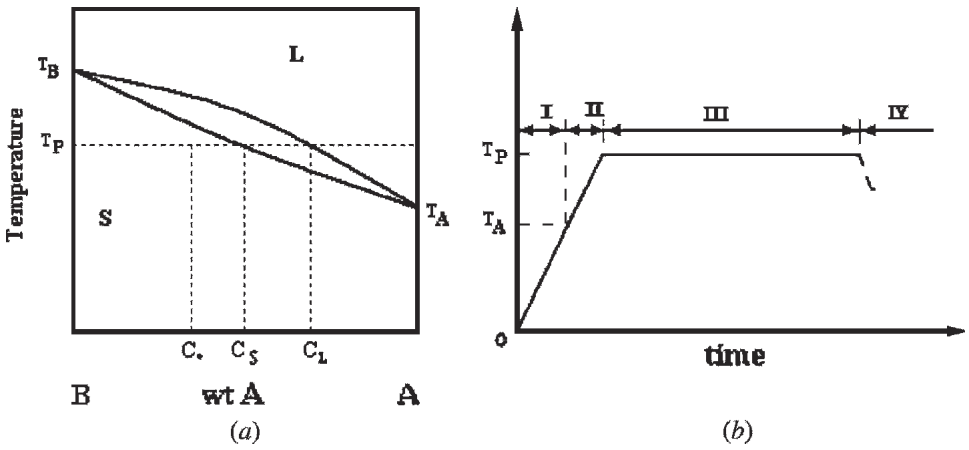

Fig. 1—Schematic equilibrium binary-isomorphous phase diagram (*a*) and typical temperature program (*b*) used in TLPS.

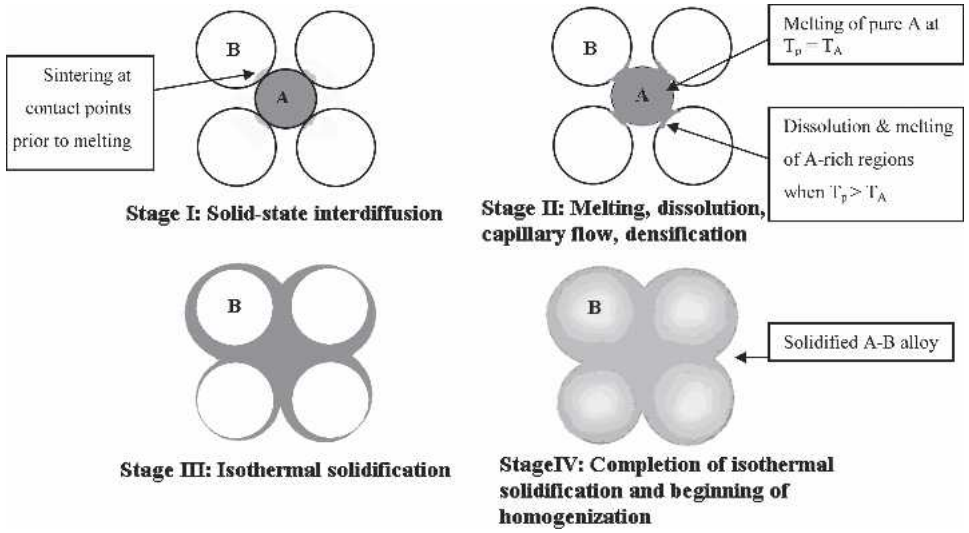

Fig. 2—Stages of TLPS.

Savitskii.[16] The dominant experimental technique used to investigate LPS in these studies was dilatometry. In this technique, the formation of a liquid phase can only be indirectly inferred by measuring the dimensional changes (or decrease/increase in density) of the sample as a function of time and temperature. In addition, little emphasis has been placed on the duration that a TLP remains in a sintered sample.

The lack of emphasis on this aspect of TLPS in previous work relates to (1) the difficulties in experimentally measuring the quantity of liquid present and (2) the facts that the primary commercial applications of TLPS to date use a relatively small amount of liquid to increase the rate of densification of a powder compact. The low liquid phase content is needed to ensure shape retention of the green part.[1] For new developing commercial applications, such as VMP solders and brazes and wide-gap TLP bonding (TLPB). joints, however, shape retention is not required or desired and higher liquid fractions are of interest. Therefore, understanding liquid formation and duration is becoming increasingly important.

Recently, an experimental technique to measure liquid phase formation directly and quantitatively has been developed using differential scanning calorimetry (DSC).[7–9] This technique has allowed the determination of initial liquid formation as well as the duration that the TLP remains in the sample (*i.e.,* the kinetics of isothermal solidification). Therefore, a model capable of predicting liquid phase formation and isothermal solidification would be a valuable tool to compare with DSC experimental results. More specifically, it is important to know the following: (1) the extent to which interdiffusion between the initial mixed powders can reduce the amount of initial liquid phase formed, (2) the impact of interdiffusion on the extent of the liquid fraction increase during dissolution, and, finally, (3) the impact that these prior processes have on the isothermal solidification kinetics during the hold segment at the T_P.

Consequently, the primary purpose of the present study was to develop a simple diffusion-based model capable of elucidating these features of TLPS. This includes an analysis of the impact of important process parameters such as

particle size, bulk mixture composition C_O, and R_H on liquid formation in the presence of solid-state interdiffusion and dissolution.

II. THE MODEL

Table I provides a summary of input and modeled parameters that are discussed in more detail below. The influence that solid-state interdiffusion can have on liquid formation during TLPS is conceptually illustrated in Figure 3. This figure shows a B/A diffusion couple at the interface of two contacting particles for the case of an isomorphous system as well as the typical solute compositional profile that forms in the solid state during heating to T_A (solid black curve). The initial base metal particle size is given by a_{Bi} and marks the location of the original interface formed before heating and interdiffusion. Once T_A is reached, only pure A regions (*i.e.,* 100 wt pct A) melt, which corresponds to a radial position of $\geq a_{Bss}$. Consequently, solid-state interdiffusion up to T_A results in an effective solid particle size increase as well as a decrease in the initial liquid fraction formed to a value of $W_{Ass} < C_O$, where C_O is the weight fraction of additive in the mixture, and therefore the amount of liquid formed in the absence of interdiffusion. If T_P increases further past T_A, a gradual dissolution of the B phase takes place, because B solubility in the liquid phase increases with increasing T_P. This is accompanied by the melting of nonequilibrium A-rich regions along the solute profile that have a A concentrations, or contents, greater than C_S (solid gray curve in Figure 3). This dissolution causes an increase in the liquid fraction formed to a value of $W_{Ao} > W_{Ass}$ and a concomitant regression of the solid/liquid interface, and the solid particle radius decreases to a_{Bo}.

W_{Ass} and a_{Bss} must be determined to account for solid-state interdiffusion and to provide accurate initial conditions for the isothermal solidification stage if it takes place at T_A. In addition, values W_{Ao} and a_{Bo} must be determined to account further for dissolution after solid-state sintering and to provide accurate initial conditions for the isothermal solidification stage if it takes place at a $T_P > T_A$. Table II lists these variables as they evolve immediately after the melting event. In a case in which no dissolution takes place (*i.e.,* isothermal solidification occurs at $T_P = T_A$), $W_{Ao} = W_{Ass}$ and $a_{Bo} = a_{Bss}$. Solute uptake from Table II is defined below.

The R_H used in the heating stage, the original B particle size, and the diffusivities of the constituents influence the gradient of the solute profile obtained and the extent of interdiffusion during solid-state sintering. This influences the degree of solid particle growth and liquid phase reduction from solid-state sintering. Heating past T_A counteracts these effects by dissolution and melt-back of the B particles. The degree of dissolution is primarily determined by T_P and R_H. The interdiffusion and dissolution process described in Figure 3 occur at every A-B contact point throughout the three-dimensional (3-D) powder mixture.

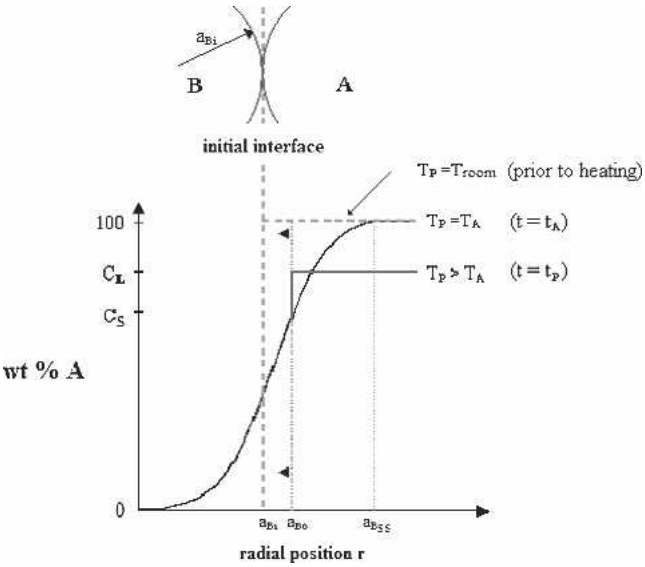

Fig. 3—Simplified schematic of solid-state interdiffusion and dissolution processes.

Table I. List of Parameters and Nomenclature

Input Parameters	Description	Values Used
D_{ol}, Q_l	Lattice diffusion parameters	D_{ol} = 5.7E-05 m^2/s Ref. [23] Q_l = 258,300 J/mol Ref. [23]
D_{ob}, Q_b	Boundary diffusion parameters	D_{ob} = 1.1E-04 m^2/s Ref. [24] Q_b = 124,700 J/mol Ref. [24]
δ	Effective grain boundary width	0.5 nm[19]
D	Base metal particle grain size	Measured experimentally
T_P	Isothermal processing temperature	1085 °C, 1140 °C, 1200 °C
a_{Bi}	Initial base metal particle size (average radius)	3.4 – 80.5 μm**
C_O	Powder mixture solute content	~65 wt pct solute
C_L	Solute solubility in liquid at T_ρ	Ref. phase diagram
C_S	Solute solubility in solid particle at T_ρ	Ref. phase diagram
Modeled Parameters	**Description**	
M_t/M_f	Fractional solute uptake by base metal at t	
W_A	Liquid fraction of A present at t	
a_B	Base metal B particle size at t	
t_C	Time for complete isothermal solidification of liquid phase	

Table II. Values of Model Parameters After Solid-State Sintering and Dissolution

Time	Processing Temperature (T_P)	Solute Uptake by B Particles (M_t/M_f)	Liquid Fraction Formed (W_A)	B Particle Size (a_B)
SS sintering complete (onset of melting)	T_A	M_{ss}/M_f	W_{Ass}	a_{Bss}
Dissolution complete isothermal solidification start)	$T > T_A$	$M_o/M_f = X_r(M_{ss}/M_f)$	W_{AO}	a_{Bo}

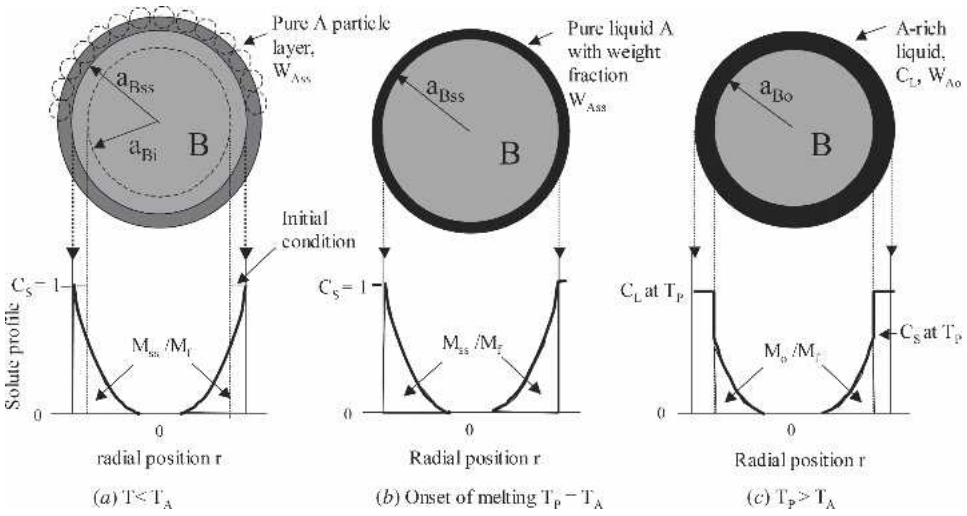

Fig. 4—Unit cells show particle size and solute distribution at different times. Note the nomenclature regions for W_A and a_B at key points in the sintering process: completion of the solid-state interdiffusion/sintering process (*a*) and initial melting and isothermal solidification at $T_P = T_A$ (*i.e.,* with no dissolution) (*b*), including dissolution attributable to heating above T_A (*c*).

Studies in TLPS of binary eutectic solder systems have led to the development of a diffusion-based model for isothermal solidification kinetics, which shows good agreement with experimental results.[8,9,17] This model did not consider interdiffusion or dissolution, however. As discussed previously, these processes are expected to be important in mutually soluble systems. Therefore, the present approach was to modify the previous model to include interdiffusion and dissolution.

The TLPS system was defined as indicated in Figures 2 and 3, where the A and B powders are mixed to a desired C_O. Under these conditions, C_O must be less than the maximum solute solubility in the solid at T_P for complete isothermal solidification of the liquid phase to be possible (*i.e.,* $C_O < C_S$ as shown in Figure 1). It is assumed that the initial condition (*i.e.,* $t = 0$, start of the isothermal stage) can be represented by the unit cell of Figure 4(a), where base metal particles, B, are surrounded by a continuous layer of additive phase, A. Interdiffusion across this couple during heating also results in the development of a solute profile in the previous B particles. Although it is a simplification of the 3-D geometry of the contact between additive and base metal particles, other studies[18,19] have indicated that surface diffusion is rapid enough that a continuous layer and supply of solute from the additive phase develop around the base metal powder early in the sintering process. For this reason, the unit cell of Figure 4(a) is considered to be a reasonable representation of the interdiffusion stage, particularly for the case in which the A powder comprises a significant fraction of the mixture and is smaller in size than the B phase. In this case, the A phase forms a matrix in which the B particles are suspended.

The initial basis of the present model has been developed in detail elsewhere[17] and is based on a mass balance of solute—in this case, element A—within the base metal particle and additive phase

$$C_O = C_A W_A + C_B W_B \quad [1]$$

where $C_A W_A$ and $C_B W_B$ are the solute contents of the additive phase and solid base metal particles, respectively; W_A and W_B are the weight fraction of each phase in the mixture; and C_A and C_B are the average solute composition of each phase. Rearrangement of Eq. [1] can give an expression for the weight fraction of additive (or liquid) phase as follows:

$$W_A = (C_O - C_B W_B)/C_A \quad [2]$$

During an isothermal hold, the composition of the additive or liquid phase is usually a constant due to rapid diffusion in the liquid. Also, assuming phase equilibria develop at the interface, C_A can be determined by the liquidus composition from the equilibrium phase diagram for a specified hold temperature (*i.e.,* C_L in Figure 1). C_O is also constant and known because it is determined by design. Therefore, knowledge of the weight fraction of the liquid during TLPS can be obtained if the solute content in the base metal (*i.e.,* $C_B W_B$) can be determined as a function of time.

A. *Solid-State Interdiffusion*

Below the melting point of pure A, we are interested primarily in how much of the additive phase remains in pure form, (*i.e.,* 100 pct solute), because this determines how much liquid is initially formed at T_A. Consequently, $C_A = 1$ before melting, and Eq. [2] simplifies to give

$$W_{Ass} = (C_O - [C_B W_B]_{ss}) \quad [3]$$

where the initial liquid fraction formed, W_{Ass}, is equal to the initial amount of pure A added to the system (*i.e.,* $W_{Ai} = C_O$) minus the amount of solute A taken up by the base metal particle B (*i.e.,* $[C_B W_B]_{ss}$ attributable to solid-state interdiffusion during the heating stage). This equation can be used to predict the weight fraction of liquid that forms initially at T_A as a result of solid-state interdiffusion, provided that an expression for $[C_B W_B]_{ss}$ can be developed.

Work by Crank[20] has led to the development of mathematical expressions and graphical solutions for the solid-state diffusion of solute through a spherical particle. Figure 4 depicts the unit cell geometry and applicable solute profiles that develop in a Crank solution. In this case, the particle is considered to be defined by a region where $0 < C_B < 1$ and the surface concentration of the particle is fixed at $C_S = C_A = 1$ (inherent in the assumption of a constant $C_S = 1$ is that there is an unlimited supply of additive phase A). Crank's analytical solution of Fick's second law of diffusion for the solute distribution within spherical particles (under the conditions shown in Figure 4 and constant diffusivity) is given by

$$\frac{C(r,t)}{C_s} = 1 + \frac{2a}{\pi r}\sum_{n=1}^{\infty}\frac{(-1)^n}{n}\sin\left(\frac{n\pi r}{a}\right)e^{-Dn^2\pi^2 t/a^2} \quad [4]$$

where a is the particle radius, r is radial position, and D is the solute diffusivity.*

*It should be noted that the diffusion profile assumed in Figure 4(b) is not equivalent to the diffusion profile expected for unlimited solubility, as described in Figure 3, because of the absence of an inflection point. This leads to a prediction that slightly overestimates interdiffusion at short times.

In the present case, the actual concentration profile within the particle is not immediately of interest. Rather, the total amount of solute that has entered the sphere (M_t) is of interest. Crank has provided the solution for fractional solute uptake (M_t/M_f), which is given by

$$\frac{M_t}{M_f} = 1 - \frac{6}{\pi^2}\sum_{n=1}^{\infty}\left(\frac{1}{n^2}\right)e^{-Dn^2\pi^2 t/a^2} \quad [5]$$

Fractional solute uptake attributable to solid-state interdiffusion can then be expressed to obtain $[C_B W_B]_{ss}$

$$M_{ss}/M_f = [C_B W_B]_{ss}/C_{Bf} W_{Bf} \quad [6]$$

where C_{Bf} is the average final composition of phase B at $t = \infty$, W_{Bf} is the weight fraction of phase B at $t = \infty$, and $C_{Bf}W_{Bf}$ is the solute content of phase B at $t = \infty$. In the Crank solution, $t = \infty$ corresponds to the time when the spherical particle is completely saturated with solute.[20] In a TLPS problem, Crank's solution is truncated at the point in time when, finally, all the solute available has been taken up and only the base metal phase remains (*i.e.,* $W_{Bf} = 1$).[17] Only when $C_O = C_S$ can the full solution for M_t/M_f be used in the isothermal solidification solution. For values of $C_O < C_S$, incomplete saturation of the particles occurs; thus, only part of the solution can be used (*i.e.,* up to a time $t < \infty$). For the case of the solid-state interdiffusion problem illustrated in Figure 4(a), $C_S = C_{Bf} = 1$, $W_{Bf} = 1$, and substitution of Eq. [6] into Eq. [3] gives

$$W_{Ass} = (C_O - M_{ss}/M_f) \quad [7]$$

As predicted by mass conservation arguments and as shown in Figure 3, solute uptake by the base metal particle is accompanied by a gradual particle growth (*i.e.,* assuming that the particle is defined by the region where $C_s < 1$). A previous study[17] has indicated that for short times and small solute uptakes during rapid heating, accounting for particle growth has only a small effect on model predictions. Therefore, a fixed initial particle size was assumed for the solid-state sintering/interdiffusion calculation in the present study.

It was decided to approximate the heat-up segment by representing this stage with an equivalent isothermal stage (in which the average diffusivity was effectively the same), because Crank's equations are for isothermal conditions. A similar approach has been used by Puckert *et al.*[11] to account for the temperature dependence of D in discrete stages. The average diffusivity of an equivalent isothermal heating stage can be obtained by calculating the arithmetic average, $\bar{D}_{eff}$, during heating from room temperature (T_o) to T_A.

$$\bar{D}_{eff} = \frac{\int_{T_o}^{T_A}(D_l(T))dT}{(T_A - T_o)} \quad [8]$$

Using $\bar{D}_{eff}$, solid-state interdiffusion was accounted for by Crank's solution for solute uptake under the conditions of the unit cell shown in Figure 4(a). Figure 4(b) illustrates the concentration profile developed in the particle at the end of the heating stage when T_A is reached. Solute uptake from solid-state sintering (M_{ss}/M_f) was then calculated using Eq. [5]. The time, t_{ss}, allowed for solute uptake is dependent on the R_H used and T_A. When the powder mixture reaches T_A, melting of the pure A regions takes place and the degree of liquid formed as a result of solid-state diffusion (*i.e.,* W_{Ass} in Figure 4(b)) can be determined by substituting the value for M_{ss}/M_f in Eq. [7].

Once this liquid forms, subsequent isothermal solidification predictions at $T_P \geq T_A$ (*i.e.,* with and without dissolution) require (1) the new particle size at T_A and (2) a method capable of taking into account the gradual particle growth during isothermal solidification. This is because the isothermal stage lasts much longer than the heating stage and involves significant solute uptake by the base metal, and thus significant changes in particle size. In this work, we adopted a previous approach[17] that developed an expression for particle growth based on solute mass conservation between the solid and liquid phases (*i.e.,* between the pure

A and B phases at T_A in the present case). This expression takes the following form:

$$a_{Bss} = a_{Bi}(W_{Bss}/W_{Bi})^{1/3} = a_{Bi}[(1 - W_{Ass})/(1 - C_O)]^{1/3} \quad [9]$$

where a_{Bi} and W_{Bi} and a_{Bss} and W_{Bss} are the base metal particle size and weight fraction initially and after heating to T_A, respectively. The mean value of a_{Bi} can be measured in the as-received powders, and W_{Bi} is simply the weight fraction of B in the bulk powder mixture, which is given by $(1 - C_O)$. Substituting these values into Eq. [9] gives the new particle size after initial heating to T_A (*i.e.,* a_{Bss}).

The effects of particle size on the initial liquid fraction formed and processing times required for complete isothermal solidification are important attributes.[2,7] These effects can be studied with the present analytical model. Predictions from Eqs. [7] and [9] for W_{Ass} and a_{Bss} (*i.e.,* expressed as normalized volumetric growth) are plotted in Figure 5 as a function of the initial base metal particle size. For ease of interpretation, the parameters used in this calculation were based on an Cu-Ni system; however, the model is applicable to any binary isomorphous system. Model input values are listed in Table I as well as in the figure captions. The value of $\bar{D}_{eff}$, given in the legend of Figure 5 was determined from Eq. [8], where D_l included a grain boundary diffusion contribution (see Section III for more detail).

These predictions show that smaller base metal particle sizes undergo greater volumetric expansion as a result of solid-state sintering. This generates smaller initial liquid formations. It is worth noting that under these conditions, particle sizes less than approximately 30 μm cause complete removal of the 100 wt pct A regions because of extensive solid-state interdiffusion. This is indicated by the prediction of no liquid formation, which makes TLPS impossible and would lead to poor densification in the powder compact during sintering. This prediction is consistent with experimental results reported elsewhere.[8] For Cu-Ni powder mixtures with 50 to 75 wt pct Cu, no liquid was formed for a Ni particle size of 3.4 μm, whereas some liquid was formed for particle sizes of 57.5 μm.[8]

In all cases in which $a_{Bi} < 30$ μm, similar volumetric expansions are shown. This is attributable to the fact that, as shown in Eq. [9], when W_{Ass} approaches 0, all the solute is taken up by the base metal powder. In the limit, each particle grows in volume representing a constant value as a result of complete uptake of the solute available (*i.e.,* $a_{ss}/a_{Bi} = [1/(1 - C_O)]^{1/3}$).

Also of interest is the effect of the R_H used to attain the desired T_P during stage I. Figure 6 shows model predictions that illustrate the relation between W_{Ass} and R_H for different particle sizes. These predictions show the following: (a) For a given initial particle size, faster R_Hs generate greater initial liquid formations by reducing the time for solid-state interdiffusion. (b) At high R_Hs, many of the predictions become asymptotic to $W_{Ass} = C_O = 0.65$ as the effects/duration of solid-state interdiffusion become negligible. (c) Smaller particle sizes require higher R_Hs to generate any liquid formation (*i.e.,* $W_{Ass} > 0$). For example, in the 30-μm prediction, an R_H greater than 40 °C per minute is required to form a liquid phase. The 3.4-μm prediction shows that R_Hs in excess of 500 °C per minute would be required to form liquid at 1085 °C.

Therefore, the model is able to indicate what R_H is necessary to form a desired liquid fraction (or any liquid at all) for a given particle size, and *vice versa*. A more thorough approach would incorporate a heat transfer analysis, particularly at higher R_Hs, which is beyond the scope of the present study, however.

B. *Isothermal Solidification Predictions at T_A*

With the liquid fraction (W_{Ass}) and particle size (a_{Bss}), it is now possible to predict the rate of isothermal solidification at T_A after the heating segment is known. Again, we adopt an approach previously used,[17] which calculates the liquid fraction present at increments of isothermal solidification time by a stepwise procedure, where $[M_t/M_f]$ is calculated by Eq. [5] and W_A is then calculated by Eq. [7]. The particle size, a_B, is then updated by Eq. [9] for the next calculation sequence after some incremental increase in time, t. The stepwise solution technique used is shown in Figure 7. Initial conditions used in this calculation are

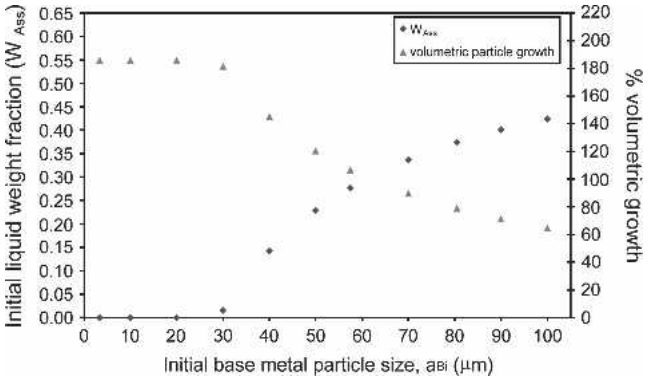

Fig. 5—Predictions of initial liquid formations (W_{Ass}) and volumetric growth of various initial base metal particle sizes (a_{Bi}). Conditions: R_H = 40 °C per minute, $T_P = T_A$ = 1085 °C, C_O = 65 wt pct Cu, and effective diffusivity (D_{eff}) = 1.2517×10^{-13} m^2/s.

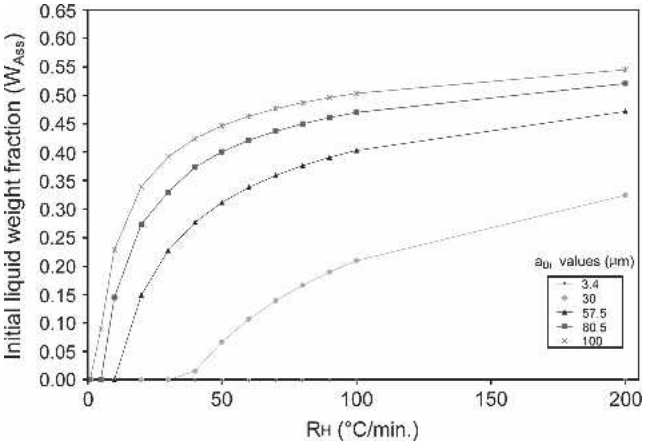

Fig. 6—Predictions of initial liquid formations (W_{Ass}) for various particle sizes and heating rates (R_Hs) during stage I. Conditions: $T_P = T_A$ = 1085 °C, C_O = 65 wt pct Cu, and effective diffusivity (D_{eff}) = 1.2517×10^{-13} m^2/s.

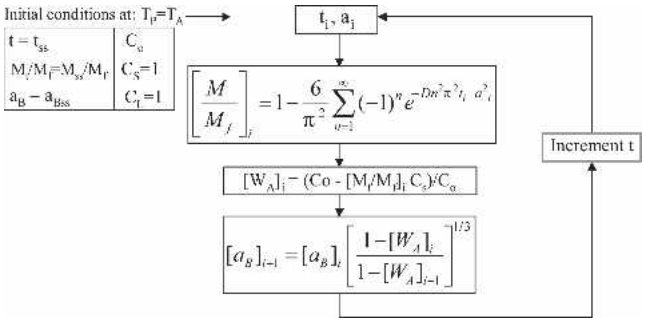

Fig. 7—Stepwise solution technique for simplified isothermal solidification kinetics model.

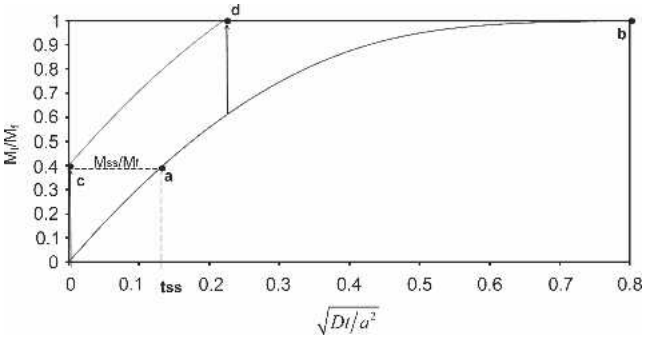

Fig. 8—Fractional solute uptake of base metal particles during isothermal solidification.

shown in the figure and represent the state immediately after heating to T_A.

To account for the solute uptake from the heating stage properly, the M_{ss}/M_f term cannot be simply inserted as a non-zero solute uptake initial condition in the stepwise solution (*i.e.,* at $t = 0$). Superimposing an amount of uptake at $t = 0$ (*e.g.*, $M_{ss}/M_f = 0.4$ as shown in Figure 8 [point c]) would artificially shift the M_t/M_f solution and cause solute uptake predictions to start at 0.4. This method gives the correct initial solute uptake at $t = 0$ but overestimates the isothermal solidification kinetics (*i.e.,* curve c to d in Figure 8), because solute uptake initially occurs at the same rate regardless of prior presaturation. To account for the partial presaturation of the base metal particles attributable to M_{ss}/M_f, it is necessary to start the M_t/M_f solution at an equivalent time (*i.e.,* t_{ss} or point a in Figure 8). This is equivalent to assuming that the solid-state solute uptake before t_{ss} occurred under the isothermal solidification conditions depicted in Figure 4(b). In this case, the proper initial solute uptake is accounted for as well as the slower kinetics of isothermal solidification caused by the ''presaturation'' of the base metal particle attributable to solid-state interdiffusion (*i.e.,* curve a to b in Figure 8).

The value of t_{ss} can be determined by solving Eq. [5] for the time variable by using the known M_{ss}/M_f, and a_{Bss} values and the remaining parameters of the isothermal solidification stage. This approach essentially solves the problem for the time it would have taken for the base metal particles to absorb M_{ss}/M_f of solute (but under the conditions of the isothermal solidification stage at T_A). The

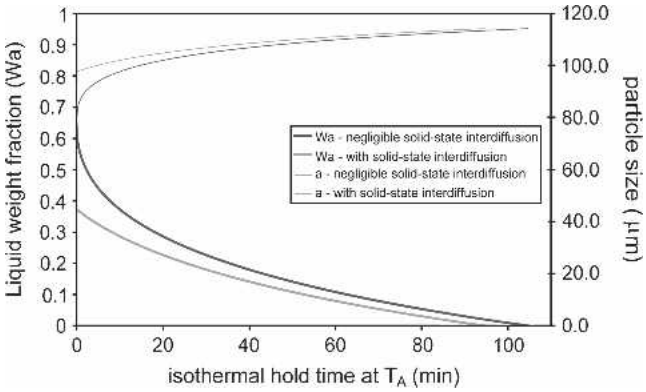

Fig. 9—Solid-state interdiffusion effects on the rate of isothermal solidification for Cu-Ni powder mixtures under these conditions: $R_H = 40$ °C per minute, $T_P = T_A = 1085$ °C, $C_O = 65$ wt pct Cu, $a_{Bi} = 80.5$ μm, and $D_{app} = 1.2517 \times 10^{-13}$ m^2/s.

remaining solute is then absorbed by solute uptake after t_{ss}. Thus, the M_t/M_f calculation must be started at t_{ss} for the beginning of the isothermal solidification stage, as indicated in Figure 7. Predictions for the isothermal solidification phase A are always plotted starting at the beginning of the isothermal stage (*i.e.,* $t = 0$ once T_P is reached).

Figure 9 illustrates two isothermal solidification and particle growth predictions for $T_P = T_A$ for two situations: (1) where solid-state interdiffusion is neglected and (2) where it is accounted for by the method discussed previously. The case neglecting solid-state interdiffusion ($M_{ss}/M_f = 0$) results in a larger initial liquid fraction that is equal to C_O and a smaller initial particle size, because no solute has been absorbed in the solid state before melting. These particles must therefore undergo a greater degree of growth to solidify the liquid isothermally *completely.* It is important to note that accounting for interdiffusion leads to less rapid isothermal solidification kinetics (indicated by a shallower slope) compared with no interdiffusion. This is attributable to the fact that interdiffusion results in larger initial base metal particles that are presaturated with solute. Despite these slower kinetic conditions, the predictions for solid-state interdiffusion indicate a slightly shorter time required for complete isothermal solidification. This is the result of a compromise between initial liquid fraction, particle size, and solute concentration profile (*i.e.,* presaturation) effects on isothermal solidification kinetics. The larger particles and shallower solute composition gradients created by solid-state interdiffusion result in slower solidification kinetics in the early stages of solidification. This is compensated for by the lower initial liquid fraction formed (W_{Ass}), however, which seems to be the dominant factor leading to shorter isothermal completion times.

Figure 10 shows the corresponding times required to complete the isothermal solidification of phase A when taking into account solid-state interdiffusion as a function of initial base metal particle size. These predictions clearly indicate that smaller a_{Bi} values generate smaller initial liquid formations (W_{Ass}), which thus require less time for removal by isothermal solidification. The presence of solid-state interdiffusion shortens isothermal solidification times compared with no interdiffusion, and this effect becomes more significant at smaller base metal particle sizes.

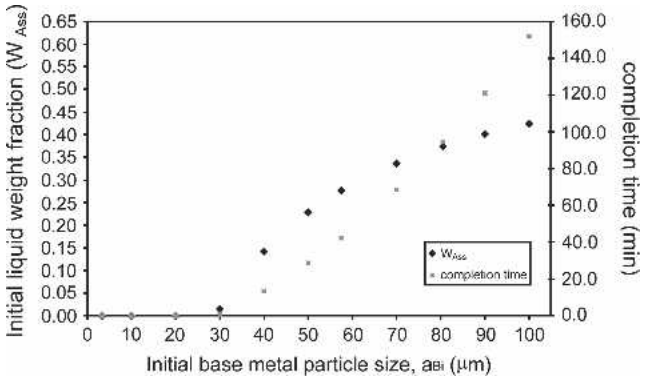

Fig. 10—Initial liquid formations (W_{Ass}) and time required for complete liquid removal for various initial base metal particle sizes (a_{Bi}). Conditions: 40 °C per minute, $T_P = T_A = 1085$ °C, $C_O = 65$ wt pct Cu, and $D_{app} = 1.2517 \times 10^{-13}$ m^2/s.

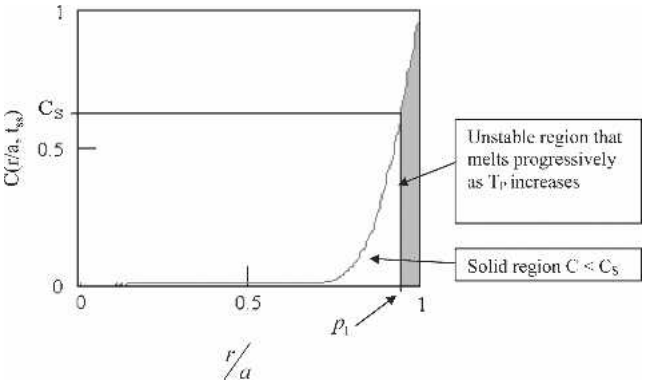

Fig. 11—Concentration profile inside the base metal particles once T_A is reached. Regions with $C > C_s$ (gray area) melt back progressively as T_P increases.

C. *Dissolution and Melt-Back Considerations for $T_P > T_A$*

For the case in which $T_P > T_A$, dissolution and melting of the outer alloyed regions of the B particle with a solute content above C_S must be accounted for. As depicted in Figure 4(c), the dissolution process increases the liquid fraction to W_{Ao} and decreases the particle size to a_{Bo}. The increase in the solubility of element B in the liquid attributable to the new equilibrium liquidus composition C_L leads to dissolution of B particles and melting of nonequilibrium alloyed regions. The surface concentration of the B particles is also reduced from $C_S = 1$ to the solidus concentration at T_P, and the solute profile in the particles is altered accordingly. It is important to note that this process causes a reduction in the solute uptake content from M_{ss}/M_f to M_o/M_f.

In the present model, B dissolution attributable to liquid solubility is accounted for by C_L now <1 (Eq. [7] and Figure 7) and melting of unstable alloyed regions is quantified by determining the concentration profile in the B particles (Eq. [4]) and identifying the nonequilibrium regions. Heating from T_A to T_P was then assumed to occur rapidly, or instantaneously. In this way, the solute concentration profile in the particle below the new C_S is unchanged from that developed during heating to T_A (*i.e.,* Figure 4(b)). This solute profile is illustrated in Figure 11, where the radial concentration $C(p,t_0)$ after solid-state interdiffusion is plotted versus the normalized particle radius, ($p = r/a_{Bi}$) for a time t_{ss} required to reach T_A. Regions having a solute content greater than C_S melt back once T_P is reached. The approximate location of the solid-liquid interface at T_P (*i.e.,* where melt-back would stop) is determined by the location at which the concentration in the solute profile is C_s (shown by the line at $p = p_1$). Regions to the right of this line melt and cause the amount of solute contained within the particle to decrease.

The amount of solute lost by the particle is represented by the area under the curve that lies to the right of the dashed line at P_1. The magnitude of this area can be obtained by integrating C from $p = P_1$ to $p = 1$. Thus, the fraction of solute remaining inside the particle (defined as X_r) can be obtained by

$$X_r = \left(\int_0^1 C(p,t_o) \cdot dp - \int_{P_1}^1 C(p,t_o) \cdot dp \right) \Big/ \int_0^1 C(p,t_o) \cdot dp \qquad [10]$$

This fraction can then be used to determine the fraction of solute uptake remaining inside the particles immediately after dissolution at T_P by

$$M_o/M_f = X_r[M_{ss}/M_f] \qquad [11]$$

where M_o/M_f is the fractional solute uptake present after dissolution and partial melt-back of the base metal particles, which initially contained M_{ss}/M_f at T_A. In the case in which $T_P = T_A$, no melt-back of the solute profile occurs ($X_r = 1$), and Eq. [11] correctly indicates that $M_o/M_f = M_{ss}/M_f$ in this case. An expression for the liquid fraction formed after dissolution can be obtained in a similar manner to that described in Eqs. [2], [5], and [7], with the primary difference being that C_A and C_B no longer equal unity but have the values of C_S and C_L, respectively. Therefore, the relevant equation becomes

$$W_{Ao} = (C_O - [M_o/M_f]C_S)/C_L \qquad [12]$$

where M_o/M_f is determined from Eq. [11]. The corresponding change in particle size from a_{Bss} to a_{Bo} at T_P can be obtained by

$$a_{Bo} = a_{Bss}[(1 - W_{Ao})/(1 - W_{Ass})]^{1/3} \qquad [13]$$

Using these new initial conditions for cases in which $T_P > T_A$, the stepwise solution of Figure 7 can then be used to calculate the rate of isothermal solidification for a case involving dissolution. Figure 12 illustrates isothermal solidification predictions of a Cu-Ni TLPS system for three different T_Ps: (1) $T_P = T_A = 1085$ °C (*i.e.,* no dissolution and melt-back), (2) $T_P = 1140$ °C, and (3) $T_P = 1200$ °C. W_A and a_B predictions are shown for each case. The initial liquid fraction predicted at $t = 0$ is greatest in the 1200 °C case, which is consistent with significant base metal dissolution and melt-back. Accordingly, this case has the smallest initial particle size, but it must grow relatively more to solidify the liquid completely isothermally. The

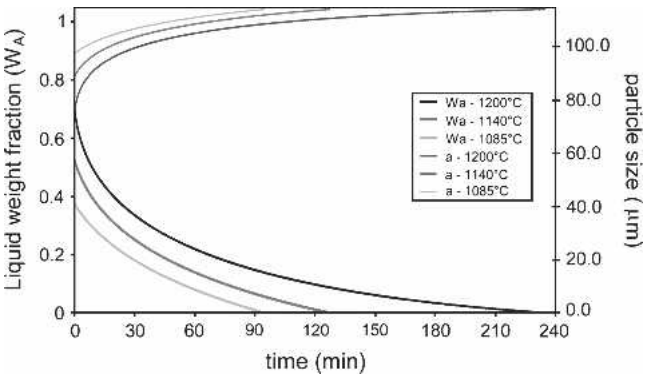

Fig. 12—T_P effects on the rate of isothermal solidification for Cu-Ni powders under conditions: R_H = 40 °C per minute, C_O = 65 wt pct Cu, a_{Bi} = 80.5 μm, T_P = 1085 °C (D_{app} = 1.2517 × 10^{-13} m^2/s), T_P = 1140 °C (D_{app} = 1.6235 × 10^{-13} m^2/s), and T_P = 1200 °C (D_{app} = 2.1978 × 10^{-3} m^2/s).

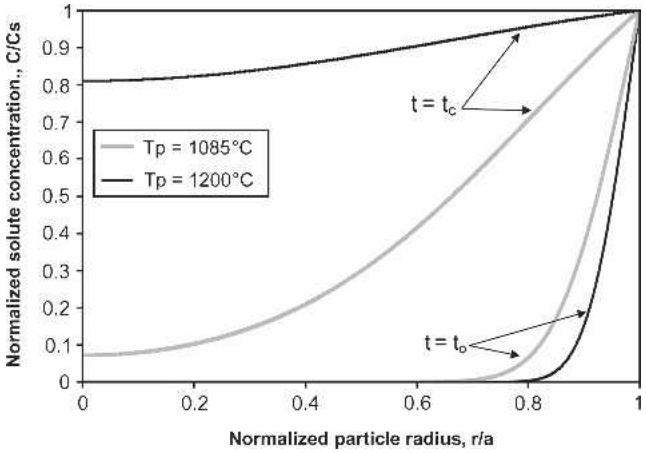

Fig. 13—Concentration profiles within B particles at beginning (t_o) and end (t_c) of isothermal solidification stage for different T_Ps: R_H = 40 °C per minute, C_O = 65 wt pct Cu, a_{Bi} = 80.5 μm, T_P = 1085 °C (D_{app} = 1.2517 × 10^{-13} m^2/s), and T_P = 1200 °C (D_{app} = 2.1978 × 10^{-13} m^2/s).

1085 °C and 1140 °C cases have initial liquid fractions of $W_{Ao} < C_O$, which indicates that base metal dissolution is not sufficient to recover the liquid lost attributable to solid-state interdiffusion. Conversely, W_{Ao} at 1200 °C is slightly greater than C_O.

A somewhat surprising result is that the time for complete removal of the liquid phase is longer at higher temperatures. This indicates that the net effect of having an increased liquid fraction from dissolution seems to dominate the kinetic effects of increased diffusivity and decreased particle size, where both would be expected to decrease solidification times.

An additional factor influencing total solidification time can be identified by noting that the slope of the predicted curves (*i.e.,* the rate of isothermal solidification) at short times increases as the T_P increases. In addition, the rate of isothermal solidification at longer times is predicted to decrease with an increase in T_P. This can be understood by referring to the predicted solute profiles in a base metal particle at the beginning (*i.e.,* after solid-state interdiffusion) and at the end of the isothermal solidification process (Figure 13).

Table III. Powder Data

Powder	Purity (metals basis)*	Size(a_{Bi})**	Shape**	Supplier
Cu	99.9 pct pure <1000 ppm oxygen	23.09 μm	Spherical	Alfa Aesar (Ward Mill, MA)
Ni	99.9 pct pure	80.5 μm	Spherical	Alfa Aesar

*Absence of contaminant phases verified via X-Ray Diffractio.
**Verified via optical microscopy, Scanning Electron Microscopy and a Horiba. CAPA-700 particle size analyzer.

At the beginning of solidification, the base metal particle contains a steeper solute profile at its surface at 1200 °C compared with 1085 °C. This is attributable to the melting back of previously interdiffused layers at $T_P > T_A$, which, together with the smaller particle size and increased diffusivity, leads to a higher initial solidification rate at 1200 °C. Conversely, near the end of the isothermal solidification time, the size of the solid particles at 1200 °C and 1085 °C is similar. In addition, the solute profile in the particle at 1200 °C is much shallower compared with that at 1085 °C. This is attributable to the fact that at 1200 °C, C_S is approaching C_O, (*i.e.,* 0.69 *vs* 0.65, respectively). Thus, the lower maximum solubility at 1200 °C requires much higher degrees of saturation (resulting in flatter/shallower profiles) to remove the liquid phase completely. A shallower concentration profile leads to the slower isothermal solidification kinetics at longer times, as clearly indicated in Figure 12 for the sample held isothermally at 1200 °C.

Figure 13 illustrates the fact that for a given bulk composition, higher T_Ps require that the base metal particle must become more saturated with solute and that a large degree of homogenization must take place in parallel with isothermal solidification. This can significantly slow down the isothermal solidification kinetics at longer times. In the extreme case, when the T_P is such that $C_S > C_O$, some liquid remains even when equilibrium is attained; thus, complete isothermal solidification of the liquid is not possible in such systems. A persistent liquid would result, and the process/system would be classified as partial transient/supersolidus LPS.[1,2]

III. COMPARISON OF MODEL WITH EXPERIMENTAL RESULTS

Recently, a method for experimentally measuring the kinetics of isothermal solidification during TLPS (in an N_2 atmosphere) has been developed using DSC, the details of which are published elsewhere.[7,9] The results for a Ni-65 wt pct Cu powder mixture (having the attributes listed in Tables I and III) are presented in Figure 14. Also shown are the predictions from the model described in Section II.

A key parameter to be used in the model is a relevant diffusivity value for a given experimental system. The work of Fisher and Rudman[18] indicates that in solid-state sintering of Cu-Ni powder mixtures, grain boundary diffusion was a dominating diffusion mechanism. Therefore, an apparent diffusivity, D_{app}, which includes the contributions

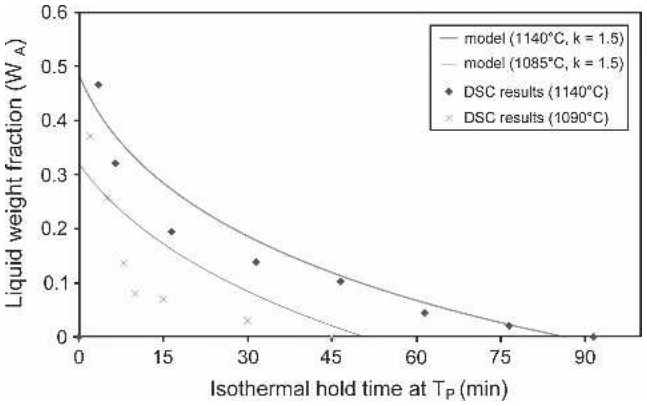

Fig. 14—The k effects on the rate of isothermal solidification for Cu-Ni powder mixtures under these conditions: $R_H = 40$ °C per minute, $C_O = 65$ wt pct Cu, $a_{Bi} = 80.5$ μm, $T_P = 1085$ °C ($k = 1.5$, $D_{app} = 2.1922 \times 10^{-13}$ m^2/s), and $T_P = 1140$ °C ($k = 1.5$, $D_{app} = 2.3511 \times 10^{-13}$ m^2/s).

of lattice and grain boundary diffusion,[9,17,21–23] was used as follows:

$$D_{app} = D_l\left[1 + k\left(\frac{\delta D_b}{dD_l}\right)\right] \quad [14]$$

where D_l is the lattice diffusivity of solute A (*i.e.,* Cu) in base metal B (*i.e.,* Ni), D_b is the grain boundary diffusivity of solute A in base metal B, δ is the grain boundary width (*i.e.,* taken to be 0.5 nm[21]), d is the average base metal grain size, and k is typically $0.5 < k < 1.5$[22] and determines the relative contribution of grain boundary diffusion to the mass transport process. The temperature dependence of D_{app} was taken into account using an Arrhenius expression and the values of D_o and Q for lattice[23] and grain boundary[24] diffusion given in Table I. Grain sizes used in the model were based on experimental measurements.[23]

Agreement between the model and experimental data are good at 1140 °C when using a k factor of 1.5, indicating a strong grain boundary contribution to the effective diffusivity of Cu diffusing in Ni. Model/experiment agreement is not as good at 1085 °C. This is partly attributable to the fact that the DSC experiments could not be carried out at 1085 °C but required some overheating to 1090 °C. Also, powder size and distribution variations, which are not included in the present model, do affect the curvature of the experimental data plots. Even at 1085 °C, however, the total time for solidification predicted by the model is close to the experimental value. The model also correctly predicts the overall trend of decreasing initial liquid fraction and time for isothermal solidification at the lower sintering temperature. The data suggest that better model/experimental agreement might be obtained at $k > 1.5$, possibly indicating even greater grain boundary contributions. This is particularly evident at lower T_Ps, where mass transport processes with lower activation energies are relatively more significant.

The remaining discrepancy that does exist between the model and experiment is primarily attributable to the difficulty in determining an appropriate value of D_{app}. This includes the value of $\bar{D}_{eff}$ as determined from Eq. [8], which is used to calculate the initial liquid formation and that calculated from Eq. [14], which is used to predict the rate of isothermal solidification. More specifically, research in the areas of diffusion-induced grain boundary migration (DIGM),[26] diffusion-induced recrystallization (DIR),[22,27–29] grain boundary grooving during TLP bonding,[30] and liquid film migration[26] has found that solute penetration and diffusion along grain boundaries occurs in many alloy systems (including Cu-Ni)[1,2,11] and often increases the rate of diffusion-based processes. Also, research by Brand and Schatt[31] has .shown that vacancy defects and their influence on the diffusion field can affect sintering rates. In addition, an important simplification made in the model is the use of intrinsic diffusivity data (*i.e.,* the dilute alloy assumption in which the diffusivity of Cu in ''pure'' Ni is assumed with no concentration dependence). In the Cu-Ni system, the concentration-dependent diffusivity increases as the Cu content increases.[18,21] Thus, the present model tends to underestimate solidification kinetics, particularly at longer times (*i.e.,* at higher Cu contents in the base metal Ni near the end of the isothermal solidification stage). It may be that incorporating these diffusion effects into the model leads to a better prediction of the experimental results, but the significant geometrical and arithmetic issues involved (*i.e.,* many interrelated parameters) are beyond the scope of the simplified analytical approach intended in this work. Their full treatment would likely necessitate a numerical modeling technique.

The incorporation of these diffusion mechanisms into model predictions and experimental verification of an appropriate D_{app} for the Cu-Ni powder systems are the subjects of ongoing work.

IV. SUMMARY AND CONCLUSIONS

A simple model was developed to predict the impact that solid-state interdiffusion and dissolution have on liquid formation and its duration during TLPS. The model predicts that solid-state interdiffusion and base metal dissolution have significant effects on the initial liquid fraction formed (W_{Ao}) and initial particle size (a_{Bo}). Solid-state alloying decreased W_{Ao} and increased a_{Bo}. Initial liquid formations were found to increase with increases in a_B and R_H by decreasing the extent of solid-state sintering.

In cases in which $T_P > T_A$, base metal dissolution counteracted the effects of solid-state sintering and caused W_{Ao} to increase and a_{Bo} to decrease. Both of these phenomena were also important in predicting the kinetics of isothermal solidification, because changes in W_{Ao} and a_{Bo} significantly influence the rate and duration of the isothermal solidification stage. The model predicted that longer times are required to solidify the greater amounts of liquid formed at higher temperatures *isothermally* (because of dissolution). This agrees qualitatively with experimental results for a Ni-65 wt pct Cu TLPS mixture sintered at 1090 °C and 1140 °C. The model also compared well with experimental results for the rate of isothermal solidification of the Ni-Cu mixture sintered at 1140 °C when a significant grain boundary diffusion mechanism was assumed. At 1085 °C, the predicted and measured total times for complete isothermal solidification were in good agreement. The rate of isothermal solidification was underestimated by the model for intermediate sintering times at 1085 °C, however.

ACKNOWLEDGMENTS

The authors thank Materials and Manufacturing Ontario (MMO) and the National Sciences and Engineering Research Council (NSERC) for their support of this work.

REFERENCES

1. R.M. German: *Liquid Phase Sintering*, Plenum Press, New York, NY, 1985.
2. R.M. German: *Sintering Theory and Practice*, Wiley-Interscience Publications, New York, NY, 1996.
3. J. Liu, A. Lal, and R.M. German: *Acta Mater.*, 1999, vol. 47, pp. 4615-26.
4. X. Qiao and S.F. Corbin: *Mater. Sci. Eng. A,* 2000, vol. A283, pp. 38-45.
5. J. McIsaac: Masters' Thesis, University of Waterloo, Waterloo, Ontario, Canada, 2001.
6. S.F. Corbin, J. McIsaac, and X. Qiao: US patent application no. 2002001260, 2002.
7. D.M. Turriff and S.F. Corbin: *Proc. 10th Int. Symp. Processing and Fabrication of Advanced Materials,* T.S. Srivatsan and R.A. Varin, eds., ASM International, Materials Park, OH, 2002.
8. S.F. Corbin and D.J. McIsaac: *Mater. Sci. Eng.*, 2003, vol. A346, pp. 132-40.
9. S.F. Corbin and P. Lucier: *Metall. Mater. Trans. A*, 2001, vol. 32A, pp. 971-78.
10. B. Reyburn and S.F. Corbin: *Int. J. Powder Metall.*, 2000, vol. 36 (5), pp. 57-69.
11. F.J. Puckert, W.A. Kaysser, and G. Petzow: *Z. Metallkd.*, 1983, vol. 74 (11), pp. 737-43.
12. T. Zhou and W.F. Gale: *Mater. Sci. Technol.*, 2003, vol. 19, pp. 1084-90.
13. W.F. Gale, X. Wen, T. Zhou, and Y. Shen: *Mater. Sci. Technol.*, 2001, vol. 17, pp. 1423-33.
14. R.M. German and J.W. Dunlap: *Metall. Trans. A*, 1986, vol. 17A, pp. 205-13.
15. R.N. Lumley and G.B. Schaffer: *Scr. Mater.*, 1996, vol. 35, pp. 589-95.
16. A.P. Savitskii: *Liquid Phase Sintering of the Systems with Interacting Components,* Russian Academy of Sciences, Siberian Branch, Institute of Strength Physics and Materials Science, Tomsk, Russia, 1993.
17. S.F. Corbin: *Metall. Mater. Trans. A*, 2002, vol. 33A, pp. 117-24.
18. B. Fisher and P.S. Rudman: *J. Appl. Phys.*, 1961, vol. 32, pp. 1604-11.
19. T. D'Hondt and S.F. Corbin: *Metall. Mater. Trans. A*, 2006, vol. 37A, pp. 217-24.
20. J. Crank: *The Mathematics of Diffusion*, Oxford Press, London, England, 1956, pp. 84-90.
21. D.A. Porter and K.E. Earterling: *Phase Transformations in Metals and Alloys*, Van Nostrand Reinhold Company, New York, NY, 1981.
22. S.M. Schwarz, B.W. Kempshall, and L.A. Gianuzzi: *Acta Mater.*, 2003, vol. 51, pp. 2765-76.
23. E.A. Brandes and G.B. Brook, eds.: *Smithells Metals Reference Book*, 7th ed., Butterworth-Heinemann Ltd., Oxford, England, 1992, pp. 13-24.
24. G.P. Grabovetskaya, I.V. Ratochka, Y.R. Kolobov, and L.N. Puchkareva: *Physics of Met. and Metallography*, 1997, vol. 83, pp. 310-13.
25. D.R. Turriff and S.F. Corbin: Presented at the 15th Canadian Materials Science Conference, June 7–10, 2003, Halifax, Nova Scotia, Canada.
26. I. Manna, S.K. Pabi, and W. Gust: *Int. Mater. Rev.*, 2001, vol. 46, pp. 53-91.
27. Y. Yamamoto, S. Uemura, and M. Kajihara: *Mater. Sci. Eng.*, 2001, vol. A312, pp. 176-81.
28. Y. Yamamoto, S. Uemura, K. Yoshida, and M. Kajihara: *Mater. Sci. Eng.*, 2002, vol. A333, pp. 262-69.
29. M. Moriyama and M. Kajuhara: *ISIJ Int.*, 1998, vol. 38, pp. 489-94.
30. N. Zhou, W.F. Gale, and T.H. North: *Int. Mater. Rev.*, 1995, vol. 40, pp. 181-96.
31. K. Brand and W. Schatt: *Z. Metallkd.*, 1993, vol. 84, pp. 893-98.